A Non-Markovian Model for the 2D Spectroscopy of Vibronic Systems.

Dale Green*[1] and Garth A. Jones[1]

[1] *School of Chemistry, University of East Anglia, Norwich Research Park, Norwich, Norfolk, United Kingdom, NR4 7TJ*

e-mail: Dale.Green@uea.ac.uk

Introduction

Ultrafast 2D spectroscopy is a valuable method for the study of condensed phase dynamics as it provides time-resolved details of both chemical structure and the interaction with the solvent environment.[1] Studies of photosynthetic reaction centres have launched the debate concerning the influence of intramolecular vibrations on the excited electronic state, inspiring the development of models where a *vibronic* Hamiltonian is introduced into an open quantum system approach.

Here, we combine a multimode vibronic model with the hierarchical equations of motion, to provide a non-Markovian treatment of the environment dynamics which correctly reproduces spectral broadening through the incorporation of long-term memory effects. Our model is applied to a perylene bisimide molecule, where two vibrational modes, $\omega_0 = 231$ cm^{-1} and $\omega_1 = 550$ cm^{-1}, contribute to the vibronic progression of the first absorption band.[2]

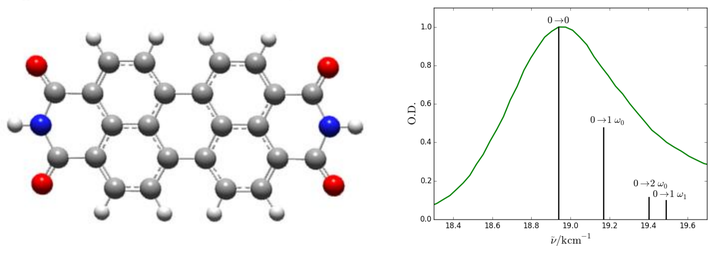

Fig. 1: (Left) Perylene bisimide chemical structure and (Right) linear absorption spectrum with labelled vibronic transitions.

Vibronic System

The model is constructed as an open quantum system, where the total Hamiltonian is separated into the contribution of the system and its interaction with a bath, representing the wider environment.

$$\hat{H} = \hat{H}_S + \hat{H}_I$$

The vibronic system consists of a ground, $|g\rangle$, and an excited, $|e\rangle$, electronic state separated by $\hbar\omega_{eg}^0$, with the two vibrational modes approximated as harmonic oscillators with the mass, m_j, frequency, ω_j, momentum, p_j, and coordinate, q_j. The excited state is displaced by d_j, corresponding to a change in its equilibrium position.

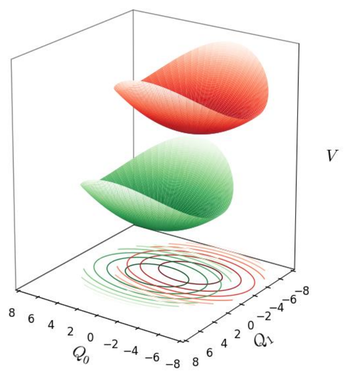

Fig 2: Potential energy surface for the two nuclear coordinates.

$$\hat{H}_S = |g\rangle \sum_{j=0,1}\left(\frac{p_j^2}{2m_j} + \frac{m_j\omega_j^2 q_j^2}{2}\right)\langle g| + |e\rangle\left(\hbar\omega_{eg}^0 + \sum_{j=0,1}\left(\frac{p_j^2}{2m_j} + \frac{m_j\omega_j^2}{2}\left(q_j - d_j\right)^2\right)\right)\langle e|$$

Bath of Harmonic Oscillators

The bath is defined as an infinite ensemble of harmonic oscillators, accounting for all the intermolecular modes which compete with the intramolecular vibrations. The coordinate of each bath oscillator, x_α, couples to the system coordinates through the operator B with strength g_α.[3]

$$\hat{H}_I = \sum_\alpha\left[\frac{p_\alpha^2}{2m_\alpha} + \frac{m_\alpha\omega_\alpha^2}{2}\left(x_\alpha - \frac{g_\alpha B}{m_\alpha\omega_\alpha^2}\right)^2\right]$$

The distribution of coupling strengths defines the spectral density, $J(\omega)$, for which we assume the Debye form.

The action of the bath is to deform the harmonic potential of the electronic excited state. This causes the vibronic transition frequencies to fluctuate, resulting in the dephasing of vibrational wave packets.

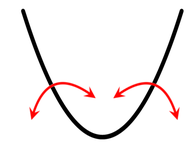

Fig 3: Diagrammatic representation of the deforming excited state potential energy surface.

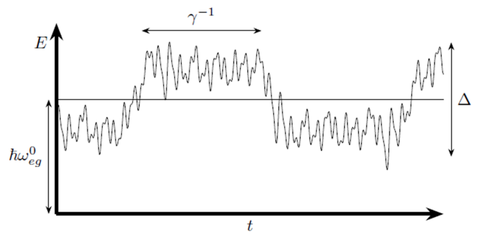

Fig 4: Bath induced fluctuation of the fundamental transition frequency.

$$J(\omega) = 2\eta\frac{\omega\gamma}{\omega^2 + \gamma^2}$$

$$\eta = \frac{\hbar\Delta^2}{2k_B T}$$

Hierarchical Equations of Motion

To a linear approximation, the system-bath coupling is related to the effective bath coordinate, X, from which we obtain the bath correlation function, $C(t)$. This can be written as the sum of exponential terms, with the Matsubara frequencies, ν_k, and coefficients, c_k.

$$\hat{H}_{SB} = BX = -\sum_\alpha g_\alpha B x_\alpha$$

$$C(t) = \langle X(t)X(0)\rangle = \sum_{k=0}^{M} c_k e^{-\nu_k|t|}$$

From the correlation function we derive an hierarchy of equations of motion, in terms of the auxiliary density operators (ADO), $\rho_{\mathbf{j}}(t)$, where $B^\times\rho$ denotes the commutator $[B,\rho]$.[4]

$$\dot{\rho}_{\mathbf{j}}(t) = -\left(\frac{i}{\hbar}\hat{H}_S^\times + \sum_{k=0}^{M}\mathbf{j}_k\nu_k\right)\rho_{\mathbf{j}}(t) - i\sum_{k=0}^{M}B^\times\rho_{\mathbf{j}_k^+}(t) - i\sum_{k=0}^{M}\mathbf{j}_k\left(c_k B\rho_{\mathbf{j}_k^-}(t) - c_k^*\rho_{\mathbf{j}_k^-}(t)B\right) - \left(\frac{2\eta}{\hbar\beta\gamma} - \eta\cot\left(\frac{\hbar\beta\gamma}{2}\right) - \sum_{k=1}^{M}\frac{c_k}{\nu_k}\right)B^\times B^\times\rho_{\mathbf{j}}(t)$$

Non-Markovianity

The Markovian limit defines the point at which the fluctuations of the bath are so much faster than the oscillations of the system, all memory of previous time steps is lost. By simultaneously propagating an hierarchy of ADOs, the memory of the bath is preserved such that information/energy transferred to the bath can be returned to the system some time later.

Each ADO corresponds to faster fluctuations, allowing the hierarchy to be terminated beyond a cut-off, Γ, defining the Markovian limit.[5]

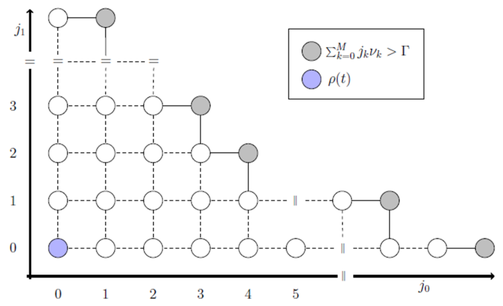

$$\frac{2(M+1)\pi}{\hbar\beta} > \Gamma \qquad \sum_{k=0}^{M}\mathbf{j}_k\nu_k > \Gamma$$

Fig 5: Structure of the hierarchy of ADOs for two Matsubara frequencies. ‖ = break in the axis, grey = terminators, blue = true density matrix.

Homogeneous vs. Inhomogeneous Broadening

Spectral broadening is a result of the speed and memory of the bath. Fast bath fluctuations cause rapid perturbations, such that individual system molecules cannot be distinguished during a measurement. This leads to an averaging across the ensemble, equivalent to the loss of memory, producing the Markovian/homogeneous limit. When the bath fluctuations are much slower, differences across the ensemble can be detected, producing an inhomogeneous distribution and a bath with a well-defined memory, requiring non-Markovian methods.[3]

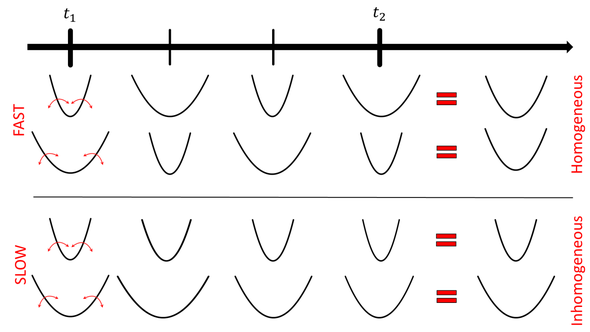

Fig 6: The origins of homogeneous and inhomogeneous broadening, shown via the change in excited state potential for two system molecules in a fast or slowly fluctuating bath.

2D Photon Echo Spectroscopy

2D spectroscopy is an ultrafast technique with sub-picosecond resolution which involves the interaction of three laser pulses, separated by the coherence, τ, and population, T, times, to generate a third order polarisation, $P^{(3)}(\tau,T,t)$, governed by the molecular response function, $\mathrm{R}^{(3)}(t_1,t_2,t_3)$.

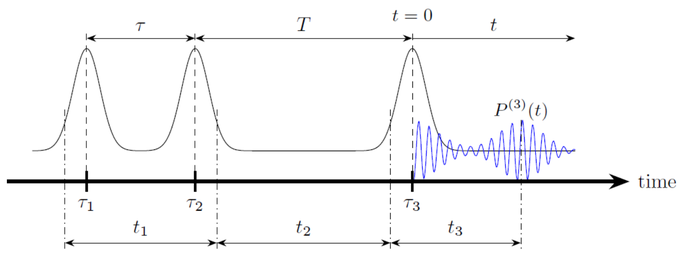

Fig 7: Pulse sequence and waiting times in 2D spectroscopy.

$$P_{\mathbf{k}_s}^{(3)}(\tau,T,t) = \int_0^\infty\int_0^\infty\int_0^\infty R^{(3)}(t_1,t_2,t_3)E(t-t_1-t_2-t_3)E(t-t_2-t_3)E(t-t_3)\mathrm{d}t_1\mathrm{d}t_2\mathrm{d}t_3$$

$$R^{(3)}(t_1,t_2,t_3) = -\frac{i}{\hbar^3}\mathbf{Tr}\left(\hat{\mu}\hat{G}(t_3+t_2+t_1,t_2+t_1)\hat{\mu}^\times\hat{G}(t_2+t_1,t_1)\hat{\mu}^\times\hat{G}(t_1,t_0)\hat{\mu}^\times\rho(-\infty)\right)$$

Fourier transform of the rephasing ($\mathbf{k}_s = -\mathbf{k}_1+\mathbf{k}_2+\mathbf{k}_3$) or non-rephasing ($\mathbf{k}_s = \mathbf{k}_1-\mathbf{k}_2+\mathbf{k}_3$) polarisation in τ, t produces a 2D spectrum for each T.

$$S_{R/NR}(\omega_\tau,T,\omega_t) = \int_{-\infty}^{\infty}dt\int_{-\infty}^{\infty}d\tau\exp[\mp i\omega_\tau\tau]\exp[i\omega_t t]iP_{\mathbf{k}_s}^{(3)}(\tau,T,t)$$

Here we enforce the impulsive limit, assuming the pulses are infinitely short, $E(t) \to \delta(t)$, where $\rho(-\infty)$ is the equilibrium density matrix, $\hat{\mu}$ is the dipole moment operator of the system and $\hat{G}(t_1,t_0)$ is the hierarchical propagator from t_0 to t_1.[6]

Spectra and line shape

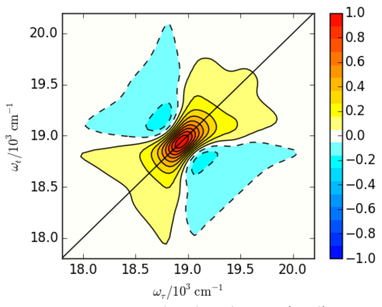

Fig 8: Normalised rephasing (real) spectrum for T = 100 fs.

2D spectra are presented as excitation, ω_τ, vs. emission, ω_t, frequency. The location of peaks provides insight into the structure of the system, whilst spectral line shape is a result of the dephasing induced by the solvent environment. Here, the bath spectral density was defined by η = 10 cm^{-1} and γ = 60 cm^{-1}.

Any inhomogeneous broadening is observed as an elongation of the peaks about the main diagonal.

Vibrational Coherences

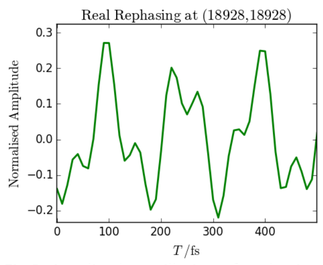

Fig 9: Amplitude oscillation of rephasing (real) for the fundamental peak.

Oscillations in the rephasing and non-rephasing amplitude with increasing population time identify coherent oscillations within the ground or excited state potential energy surface, corresponding to the intramolecular vibrations of the system.

A third Fourier transform over T allows the frequencies contributing to these oscillations to be separated and plotted as amplitude spectra.[4]

Amplitude Spectra

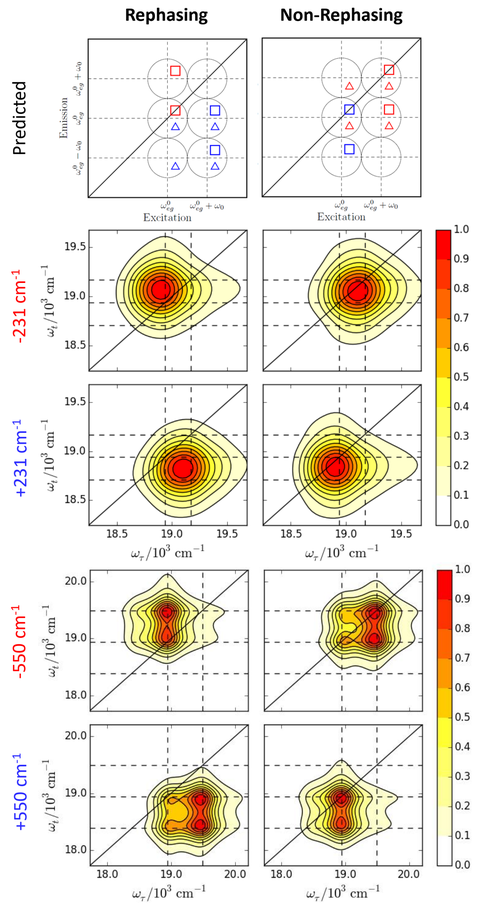

Analysis of all the Liouville pathways predicts a 'chair' arrangement of peaks, which can be observed for both vibrational modes.[4]

The third Fourier transform separates positively, $e^{+i\omega_0 T}$, and negatively, $e^{-i\omega_0 T}$, oscillating pathways.

Fig 10: Predicted peak location diagrams and amplitude spectra for the two vibrational modes, separated into positive (blue) and negative (red) oscillations for the rephasing (left) and non-rephasing (right) spectra. Triangles and squares correspond to ground state bleach and stimulated emission coherence pathways, respectively.

Summary

Here, we have developed a rigorous vibronic model evolved within a non-Markovian bath and have shown how the contributions of the system and environment can be studied separately using 2D spectroscopy. This research was carried out on the HPC Cluster supported by the Research and Specialist Computing Support service at UEA.

Future Research

Further development is already underway, including:

- Extension to vibronic dimer systems and larger aggregates.
- Quantification of non-Markovianity and an analysis of its relationship with the limits of spectral broadening.
- Inclusion of multi-coloured, variably polarised laser pulses.

References

1) M. K. Petti, J. P. Lomont, M. Maj and M. T. Zanni, *J. Phys. Chem. B*, 2018, **122**, 1771–1780.
2) A. E. Clark, C. Qin and A. D. Q. Li, *J. Am. Chem. Soc.*, 2007, **129**, 7586–7595.
3) Y. Tanimura, *J. Phys. Soc. Jpn.*, 2006, **75**, 082001.
4) D. Green, F. V. A. Camargo, I. A. Heisler, A. G. Dijkstra and G. A. Jones, *J. Phys. Chem. A*, 2018, **122**, 6206–6213.
5) A. G. Dijkstra and V. I. Prokhorenko, *J. Chem. Phys.*, 2017, **147**, 064102.
6) Y. Tanimura, *J. Chem. Phys.*, 2012, **137**, 22A550.